Solid State Communications 370 (2023) 115229

Contents lists available at ScienceDirect

Solid State Communications

journal homepage: www.elsevier.com/locate/ssc

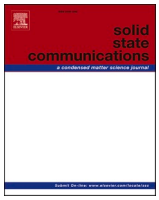

First principles study of the structural, half-metallic ferromagnetism, magnetic, and transport properties of KXO_2 (X = Pr, Nd, and Pm) hexagonal oxides

Bisma Tariq [a], G. Murtaza [b,**], Hassan Ali [c], Samia Razzaq [b], R.M. Arif Khalil [d,***], Muhammad Iqbal Hussain [e,*], Khawar Ismail [b,c], Ghazanfir Nazir [f], Nouf H. Alotaibi [g]

[a] Istituto Italiano di Tecnologia (IIT) Center for Bionanotechnologies, 1-73010, Arneseno, Italy
[b] Centre for Advanced Studies in Physics GC University Lahore, 54000, Pakistan
[c] Department of Physics, University of Narowal, 51600, Pakistan
[d] Materials Simulation Research Laboratory (MSRL), Department of Physics, Bahauddin Zakariya University Multan, 60800, Pakistan
[e] Department of Physics, University of Education, Lahore, 54000, Pakistan
[f] Department of Nanotechnology and Advanced Materials Engineering, Sejong University, Seoul, 05006, South Korea
[g] Department of Chemistry, College of Science, King Saud University, P.O. Box 22452, Riyadh, 11451, Saudi Arabia

ARTICLE INFO

Communicated by Ralph Gebauer

Keywords:
Half metallicity
Magnetic properties
Transport properties
WIEN2K

ABSTRACT

The density functional theory (DFT) studies are made to calculate the electronic, magnetic, and transport characteristics of potassium lanthanide KXO2 (X = Pr, Nd, and Pm) oxides have been studied by using the WIEN2K code. Perdew Burke Ernzerhof-Generalized Gradient approximation (PBE-GGA) is used for the exchange-correlation energy of the crystal structures in the hexagonal phase. However, the volume-optimized graphs depict that these compounds are energetically stable in the ferromagnetic state. Moreover, the studies of the spin-up channels of the band structure and density of states (DOS) reveal their metallic behavior whereas semiconductor nature has been noticed through spin-channels. Therefore, studied materials have half metallicity nature with 100% spin polarization at the Fermi level (EF). Total and partial magnetic moments of KXO2 (X = Pr, Nd, and Pm) and individual atoms exist due to unpaired 4f electronic states of the lanthanide ions, present at the EF. The energy difference between anti-ferromagnetism and ferromagnetism versus the volume optimization curve gives the curie temperature (Tc). The volume optimization curves show a flat region where both magnetic states have similar energies. This means the material can exist at the equilibrium volume in either state. Finally, thermoelectric properties are calculated by the BoltzTraP code. Our results unveil that these potassium-based lanthanide oxides are potential materials for devising spintronics devices and lifting future practical applications.

1. Introduction

Nowadays, the development in the miniaturization of commercial electronic devices has reached its physical limits. Still, an intensive effort is required to replace the recent silicon technology, based on the electric current (charge) as the primary information carrier, with a new model that provides a faster and more energy-efficient transport and processing of information as compared to ordinary electronic devices. One of the best promising possibilities is to utilize electron spin (spin current) as an information carrier, a keystone of spin electronics (spintronics), a rapidly growing branch of material physics. The spintronic devices are fabricated by ferromagnetic materials where the information is transported in the form of spin current, and spin waves [1]. Therefore, Half Metallic Ferromagnetic (HMF) materials are deemed potential ones for spintronics applications. Half metallic semiconductor materials are types of magnetic materials that depicted unique characteristics due to imbalanced spin at E_F for the spin-up and spin-down channels. This way, conduction comes from charge carriers (electrons) only through one spin channel. These spin-based semiconductor materials have offered several advantages over nonmagnetic materials [2].

* Corresponding author.
** Corresponding author.
*** Corresponding author.
E-mail addresses: gmrai@gcu.edu.pk (G. Murtaza), muhammadarif@bzu.edu.pk (R.M. Arif Khalil), miqbal@ue.edu.pk (M. Iqbal Hussain).

https://doi.org/10.1016/j.ssc.2023.115229
Received 18 March 2023; Received in revised form 24 May 2023; Accepted 26 May 2023
Available online 27 May 2023

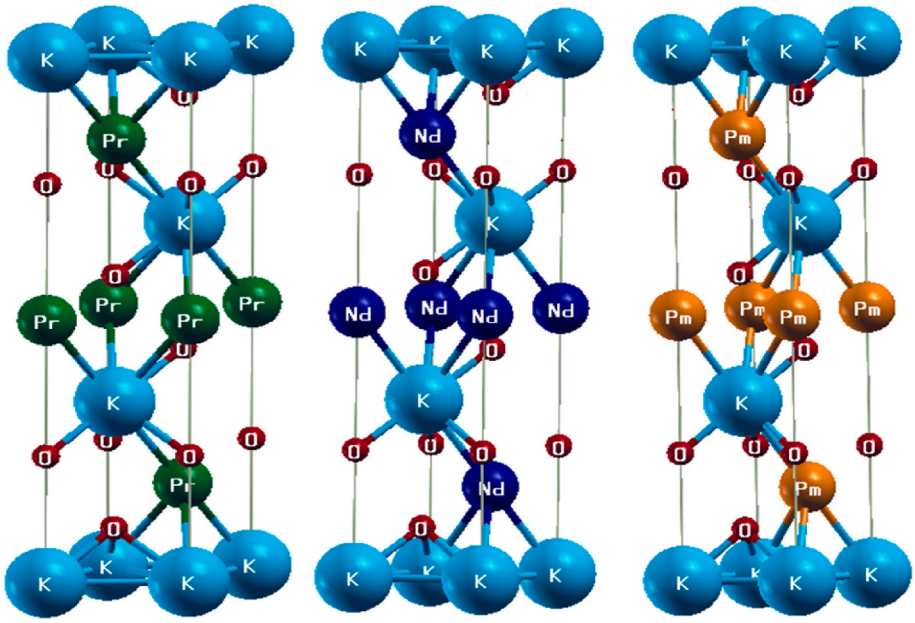

Fig. 1. Hexagonal crystal structure of $KPrO_2$, $KNdO_2$, and $KPmO_2$.

Moreover, low T_c and sustainability of the spin injection in magnetic materials is one of the burning questions in spintronics [1]. Therefore, the discovery of ternary alloy HMF materials become an attractive interest for researchers of the era [3]. These materials offer higher T_c, and maximum spin polarization and have a wide range of applications in the field of spintronics and optoelectronic and thermoelectric devices [4]. These unique properties of HM show 100% spin polarization near E_F [5,6]. HMF has a low magnetic moment, low magnetization, less stray field, and small energy loss, which is not affected by the strong external magnetic field. These fascinating properties of HMF make them a potential candidate for enhancing the working efficiency of the spintronics [3,6].

In the past decades, theoretical studies have been performed on HMF materials for exploring novel magnetic semiconductor materials to enhance efficiency of the spintronics devices. Hachimi et al. [7] interpreted the half-metallic as well as magnetic properties of rare earth elements atoms doped in ZnO by WIEN2K software based on DFT. Similarly, Yaqoob et al. [4] have also predicted the half-metallicity and thermoelectric properties of $XMnTe_2$ (X = Li, Na, K) by using DFT. Moreover, Chepkoech et al. [8] performed the *ab-initio* calculations for thermoelectric properties of $XCuO_2$ (X = K, Rb, Cs) by VASP package and discussed the efficiency of these materials by finding the figure of merit (ZT). Likewise, Bin Dong et al. [9] have reported an experimental study for the crystal structure, magnetic susceptibility, and heat capacity of ternary potassium lanthanide oxides. Benmakhlouf et al. [10] explored the half-metallic ferromagnetism in $KMnQ_2$ (Q = O, S, Se, Te) by plane-wave pseudopotential total energy system as implemented within the CASTEP package. Similar studies exist and have formerly been reported to explore various physical properties for their potential applications in a diverse range of optoelectronic, thermoelectric, and spintronics devices [11–16].

Since the lanthanide oxides show sufficient magnetic moment owing to higher localized electronic states of *f*-orbitals. The magnetic interaction between *f*-orbital with *s- and p-* orbitals is very weak as compared to *d*-orbital electrons. As per literature, heretofore, no literature is found to be available for comparing the structural, half metallicity, and magnetic properties of potassium-based lanthanide oxides, i.e., KXO_2 (X = Pr, Nd, and Pm) for various thermoelectric and spintronic applications. Therefore, we are hereby motivated to investigate the structural, half metallicity, and magnetic behavior of novel material, i.e., KXO_2 (X = Pr, Nd, and Pm). To calculate the accurate exchange-correlation potential of these oxides, we have used the PBE + GGA approximation. The half-metallicity and magnetic response of these compounds are checked by performing the spin calculation within the DFT approach [17,18].

2. Computational methodology

The first principles study of the structural, half metallicity, and magnetic characteristics of potassium lanthanide oxides KXO_2 (X = Pr, Nd, and Pm) are investigated by spin-polarized DFT calculations [19,20]. All spin-polarized DFT calculations are based on a full potential-linearized augmented plane wave plus local orbital (FP-LAPW + Lo) system. FP-LAPW + Lo system relay on the many-body system of quantum mechanics within the WIEN2k code. The PBE + GGA approximation scheme is used to investigate the exchange-correlation potential energy of the studied materials [21]. The unit cell volume was distributed in two regions; the muffin-tin radius and the interstitial region. FP-LAPW + Lo was also used to demonstrate the electronic behavior in the internal side of the muffin tin (R_{MT}) sphere and the interstitial region. For spin-polarized calculations, the wave function's angular momentum inside the atomic spheres expands up to $L_{max} = 10$. The selection of suitable R_{MT} values plays a potential role to prevent the leakage of the current of core electrons. The selected values of muffin tin radii (R_{MT}) for individual potassium atoms (K), Lanthanide atoms, and oxygen atoms (O) are 1.65, 2, and 1.5 (Bohr), respectively. In addition, the plane wave cut-off parameters value is the product of the muffin-tin radius sphere and largest reciprocal lattice vector; its value is selected as $R_{MT} \times K_{max} = 10$. A k-mesh of 500 points was taken in the first Brillouin zone (BZ). In addition, the value of Gaussian factor G_{max} opts as 16 and -9.0 R y energy has been chosen for the separation between the core electronic states and valence electronic states.

3. Results and discussion

3.1. Structural properties

The crystal structure of potassium lanthanide oxides KXO_2 (X = Pr, Nd, and Pm) have been optimized in the hexagonal phase with space group (166_R-3m), and their unit cell crystal structures are depicted in Fig. 1. To calculate the lattice parameters, bulk modulus and to draw the

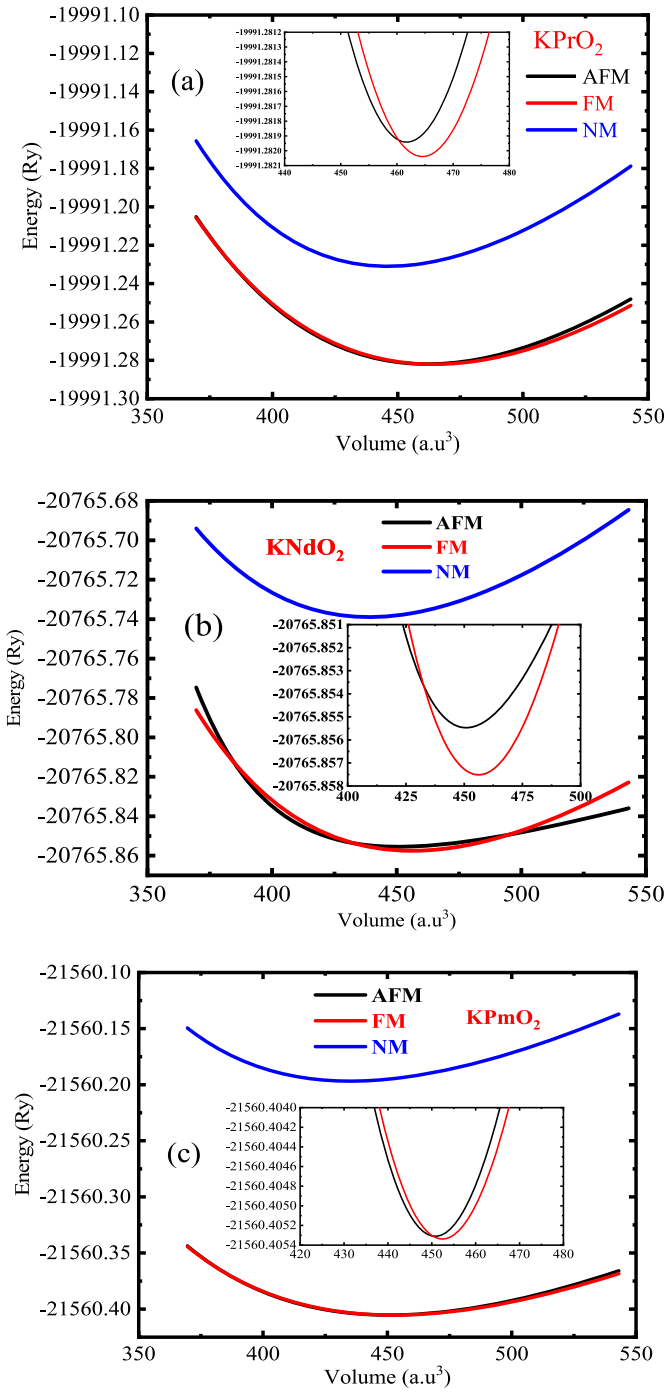

Fig. 2. Ground state energy as the function of volume (a.u^3) for (a) $KPrO_2$ (b) $KNdO_2$ (c) $KPmO_2$ in FM, AFM, and NM phases.

Table 1
The lattice parameters a, b & c (Å), Bulk modulus B (GPa), bandgap E_g (eV), and formation energy ΔE_f of potassium lanthanide oxides KXO_2 (X = Pr, Nd and Pm).

Compounds	a = b(Å)	c(Å)	B	E_g	ΔE_f	T_c (K)
$KPrO_2$	4.18[a,b]	18.04[b]	89.05	2.62	−2.91	282
$KNdO_2$	4.23[a,c]	18.17[c]	89.74	3.34	−2.95	305
$KPmO_2$	4.29[a,b]	18.26[a]	86.89	4.00	−2.98	295

Ref. [9][a].
Ref. [22][b].
Ref. [23] [c].

volume optimization curve, we used Birch-Murnaghan isothermal equation of state [2]. The ferromagnetic (FM), antiferromagnetic (AFM), and non-magnetic (NM) volume-optimized curves are plotted between energy in (Ry) versus volume (a.u^3). From Fig. 2; it is observed that all studied compounds offer minimum ground state energy for FM states [7]. Moreover, to ensure room temperature ferromagnetism, we have calculated the T_c by using the Heisenberg model such as $T_c = 2\Delta E/3x\ K_B$, here ΔE is the difference between AFM and FM energy states, x represents the number of lanthanide atoms in compounds, and K_B is the Boltzmann constant [21]. The lattice parameters (Å), Bulk modulus B (GPa), bandgap E_g (eV), and formation energy (ΔE_f) are listed in Table 1. The values of the lattice parameters determined for KXO_2 (X = Pr, Nd, and Pm) are consistent with the formerly reported experimental [9] and theoretical results [22,23]. The negative value of ΔE_f for these compounds shows that these are energetically sustainable [24] compounds.

3.2. Half metallic ferromagnetism

The spin-polarized electronic behavior of potassium lanthanide oxides KXO_2 (X = Pr, Nd, and Pm) has been analyzed along high symmetry points, i.e., Γ, H, N, and P in the first BZ. Fig. 3(a–c) represents the spin-polarized band structures of KXO_2 (X = Pr, Nd, and Pm) compounds which unveil that all these three compounds show metallic behavior for the spin-up channel, whereas a significant forbidden energy gap has been noticed through their spin-down states, leading to the semiconducting nature of these materials. The considered compounds have shown a direct band gap semiconducting nature [25,26]. The band gap value in the spin-down channels of these compounds is noted as 2.62 eV for $KPrO_2$, 3.34 eV for $KNdO_2$, and 4.0 eV for $KPmO_2$. These values are listed in Table 1. The increase in energy band gap from Pr < Nd < Pm follows the similar anomaly that occurred in their ionic radii. Generally, in HMF materials, the conduction of spin electrons with charge comes through one spin channel only. So, the spin channels have shown half-metallic ferromagnetism (HMF) [2,4]. It is anticipated that the presence of lanthanide ions in these oxides might be responsible for their HMF behavior. HMF materials are considered a potential candidate for spintronic applications.

The atomic orbital electronic states of the studied compounds can be understood by calculating the total densities of states (TDOS) and partial densities of states (PDOS). The results describing the DOS of KXO_2 (X = Pr, Nd, and Pm) can be visualized through Fig. 4(a–c). It is noticed through pictorial views of the TDOS and PDOS that electronic energy states for the majority spin-up channel and minority spin-down channel are unsymmetrical around the E_F. For the spin-up channel, the electronic states of potassium, oxygen, and lanthanide atoms are seen overlapping at E_F depicting metallic behavior. While, spin down channel shows semiconductor behavior due to a significant energy band gap between the electronic states of potassium, oxygen, and lanthanide atoms present in the VB and CB. In addition, *f*-orbitals of X ions are found to be hybridized with the *s*-orbital of potassium atoms and *p*-orbitals of oxygen atoms in the VB and CB. It can further be noticed through Fig. 4(a–c) that electronic energy states of *f*-orbitals contributed maximally as compared to the *p*-orbitals of X ions and oxygen atoms. It is probed furthermore that one spin is contributing mainly to the conduction mechanism in all compounds. For spintronics devices, spin control has been a major challenge to the researchers of this era. Therefore, these half-metallic materials may resolve the issues about the spin control and may have the ability to offer 100% spin polarization near E_F. The spin polarization can be calculated by the following relation [2,4].

$$P = \frac{N_\uparrow(E_F) - N_\downarrow(E_F)}{N_\uparrow(E_F) + N_\downarrow(E_F)} \quad (1)$$

Here, $N_\uparrow(E_F)$ and $N_\downarrow(E_F)$, are the number of up spins, and down spins across E_F, respectively. So, spin can be sustained and controlled while using HMF materials for spintronics applications. The results obtained through the spin-polarized band structures and DOS are found to be

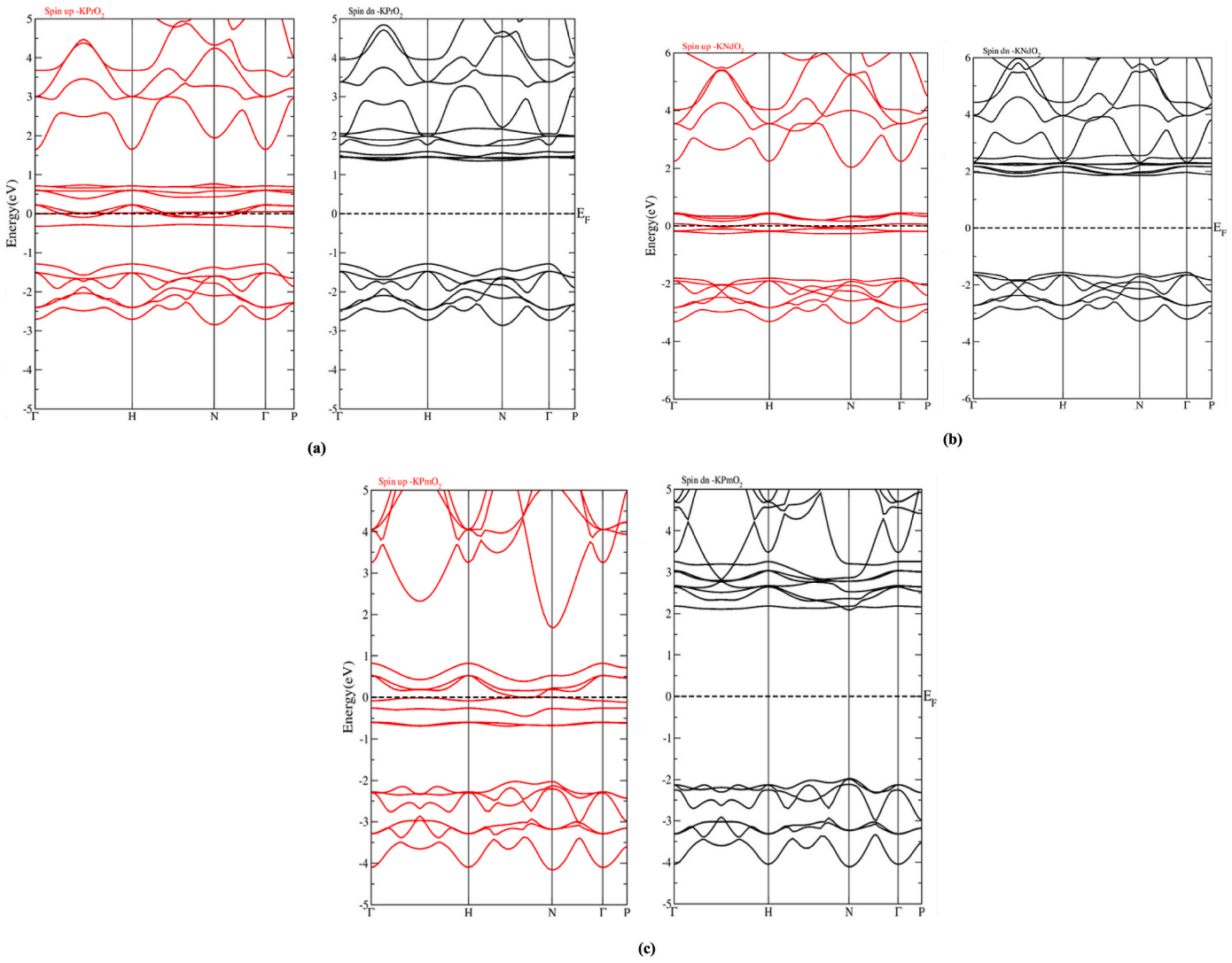

Fig. 3. (a): The spin-polarized band structure of $KPrO_2$.
Fig. 3 (b): The spin-polarized band structure of $KNdO_2$.
Fig. 3(c): The spin-polarized band structure of $KPmO_2$.

consistent with each leading to the viewpoint that these compounds have confirmed half-metallic ferromagnetism.

3.3. Magnetic properties

In this sub-section, the crystal field splitting mechanism of the electronic distributions *f*-states of X ions into three parts consisting of t_{1g}, t_{2g} (the highest three folds degenerate energy states), and a_{2g} (the lowest single-fold degenerate energy state) as explored by John Teller distortion [27,28]. The degeneracy of these energy states is shown in Fig. 5 (a–c). The crystal field theory has demonstrated the splitting of *f*-orbital energy states of lanthanide ions, which are found to be responsible for the occurrence of the magnetic moment in these compounds [7,29]. For rigor, it has been observed that during the hybridization mechanism, oxygen ions approached the lanthanide ions, i.e., (X = Pr, Nd, and Pm) by octahedral environment and split into seven electronic states of 4*f*-orbitals. In response to the splitting of *f*-orbitals energy states, the magnetic moment is produced at sites of various atoms and interstitial sites that are present in the unit cell. The magnetic moment noted for KXO_2, K, X, and O atoms is presented in Table 2. PDOS unveils that the magnetic moment of potassium and oxygen atoms comes from the hybridization between the *s*-orbital of K and *f*-orbital of lanthanide atoms (*s-f*) and *the p*-orbital of oxygen atoms and *f*-orbital of lanthanide atoms (*p-f*).

In addition to the above, during the bonding formation, rare earth metal atoms donate three electrons to the oxygen atoms. The splitting of quantum electronic states and electronic configurations of these lanthanide ions are f^2, f^3, and f^4 as depicted in Fig. 5(a–c) [7]. The electronic configurations of these compounds have depicted that magnetic moment has occurred due to the availability of unpaired electrons and splitting of the orbital states of lanthanide ions, i.e., (X = Pr, Nd, and Pm). The total magnetic moment of these compounds is an integer form that endorses half metallicity [2,4,30].

3.4. Transport properties

BoltzTraP code is based on the semi-classical Boltzmann theory used to calculate the thermoelectric properties of the materials within the DFT framework. These properties are based on the electronic band structure of the materials [31]. The materials, which are found to have good thermoelectric properties, are used to convert squandered heat energy into useful electrical energy. Such materials are widely being used to devise spin caloritronic devices, which is a new emerging research field that has been introduced as a novel way for generating

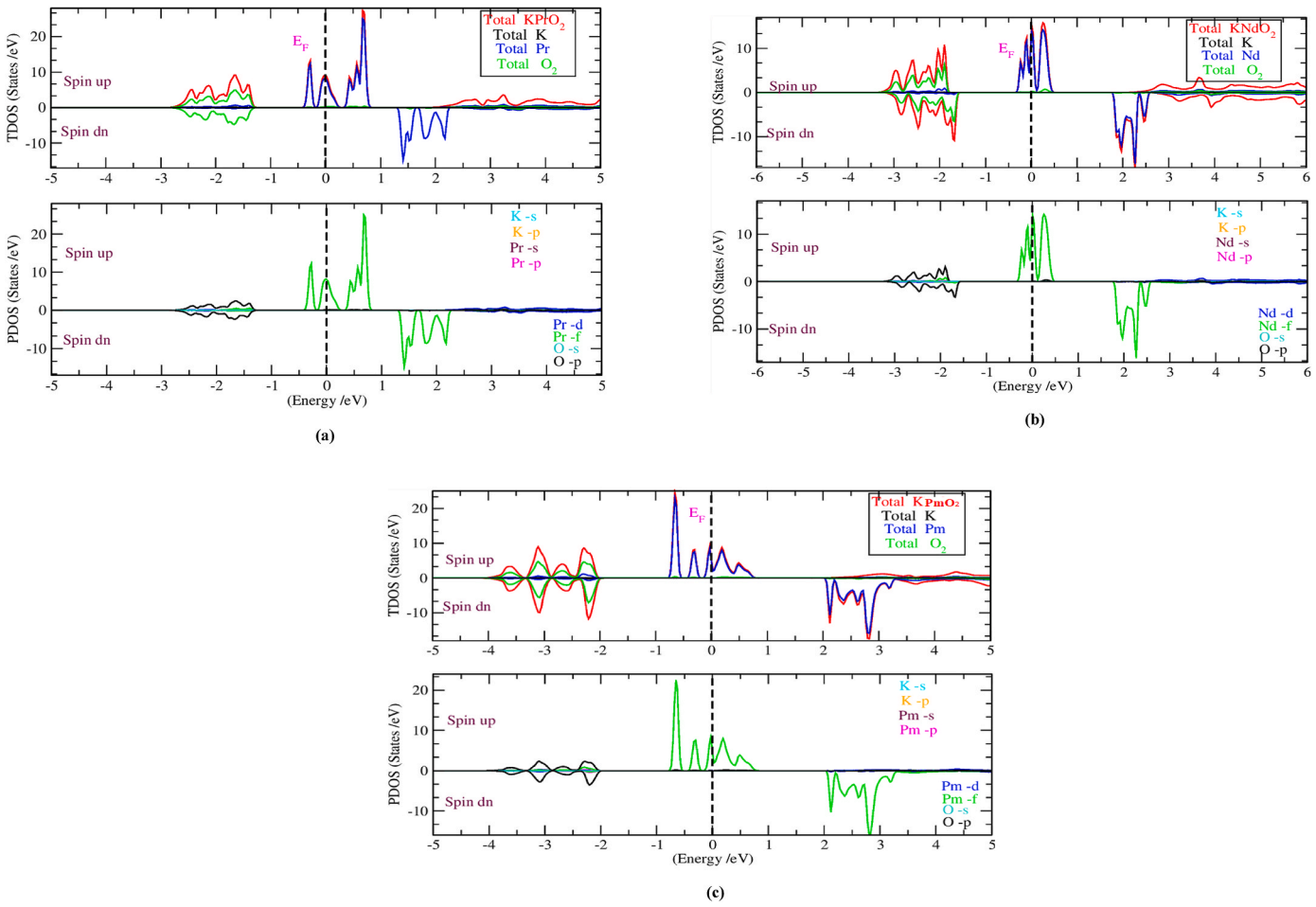

Fig. 4(a). Spin-based total and partial density of states of $KPrO_2$.
Fig. 4(b): Spin-based total and partial density of states of $KNdO_2$.
Fig. 4(c): Spin-based total and partial density of states of $KPmO_2$.

heat current valves [32]. Moreover, the demand for green energy is increasing globally which may be fulfilled by using spin caloritronic and thermoelectric materials. Therefore, thermoelectric devices are widely utilized in power generation for the production of electricity by coal energy. Temperature-dependent parameters like electrical conductivity (σ/τ), Seebeck coefficient (S), Hall coefficient (R_H), Thermal conductivity (κ/τ), heat capacity (C_v), magnetic susceptibility (χ), and ZT have a significant role to explain the transport behavior of any semiconductor materials [33]. Where the ZT parameter is capable enough to explain the efficiency of thermoelectric devices [2,34,35]. In this regard, the thermoelectric properties of KXO_2 (X = Pr, Nd, and Pm) are studied in the temperature range (100 K–800 K).

The electrical conductivity is computed by using the relation ($\sigma = \mu ne$) [1,2]. The σ of semiconductor materials depends upon the mobility (μ) of charge carriers and concentration of charge carriers (ne). Although, when the number of charge carriers and mobility increases then the electrical conductivity shows its inverse relationship with the increment of thermal agitation. The electrical conductivity plots for KXO_2 (X = Pr, Nd, and Pm) are depicted in Fig. 6(a). It is observed that initially, electrical conductivity is higher for $KPrO_2$ and $KNdO_2$ from 100 K to 200 K, which however, starts decreasing beyond this specific limit of 200 K–800 K temperature due to variations of band gap values and thermal agitation process. $KPmO_2$ has depicted linear behavior with the temperature due to its higher band gap.

The Seebeck coefficient (S) is associated with the thermoelectric voltage across the ends of the semiconductor materials. The thermoelectric voltage arises due to the difference of temperature across the ends of materials accordingly to this relation $S = -\Delta V/\Delta T$ [36]. Fig. 6(b) shows the Seebeck coefficient of the studied compounds. It is observed that the thermoelectric voltage is generated due to the negative charge carriers. The S of $KPmO_2$ and $KNdO_2$ shows higher values with variation of temperature as compared to $KPrO_2$, due to variation of band gap values and easy movement of charge carriers from VB to CB within materials. This causes to induce a thermoelectric voltage across the studied materials. Furthermore, the KmO_2 band gap value is 4.0 eV, therefore the movement of charge carriers from VB to CB is less and the temperature difference is higher across $KPmO_2$ than the other two semiconductors, i.e., $KNdO_2$ and $KPrO_2$. Hence, $KPmO_2$ shows a higher value of Seebeck coefficients.

The temperature-dependent Hall coefficient determines the type of charge carriers in semiconductor materials, either the materials have *n*-type charge carriers or vice versa [37]. Fig. 6(c) depicts the variation of the Hall coefficient of these materials. It has been noticed that its value for $KPrO_2$ is shifted from a negative value to a positive one with a variation of temperature (100 k to 800 K). So, $KPrO_2$ shows the *n*-type semiconductor nature from 100 K to 400 K. After that, it becomes positive showing *p*-type behavior owing to phase shifting. Whereas, $KNdO_2$ has depicted a positive value of Hall coefficient throughout the temperature range from 100 K to 800 K leading to the fact that it is a *p*-type semiconductor. In the case of $KPmO_2$, the negative charge carriers are dominant so, its negative Hall coefficient recognizes it as an *n*-type semiconductor.

The thermal conductivity can be computed by Wiedemann-Franz law such as $k = L\sigma T$ [3]. Fig. 7(a) shows the behavior of the thermal

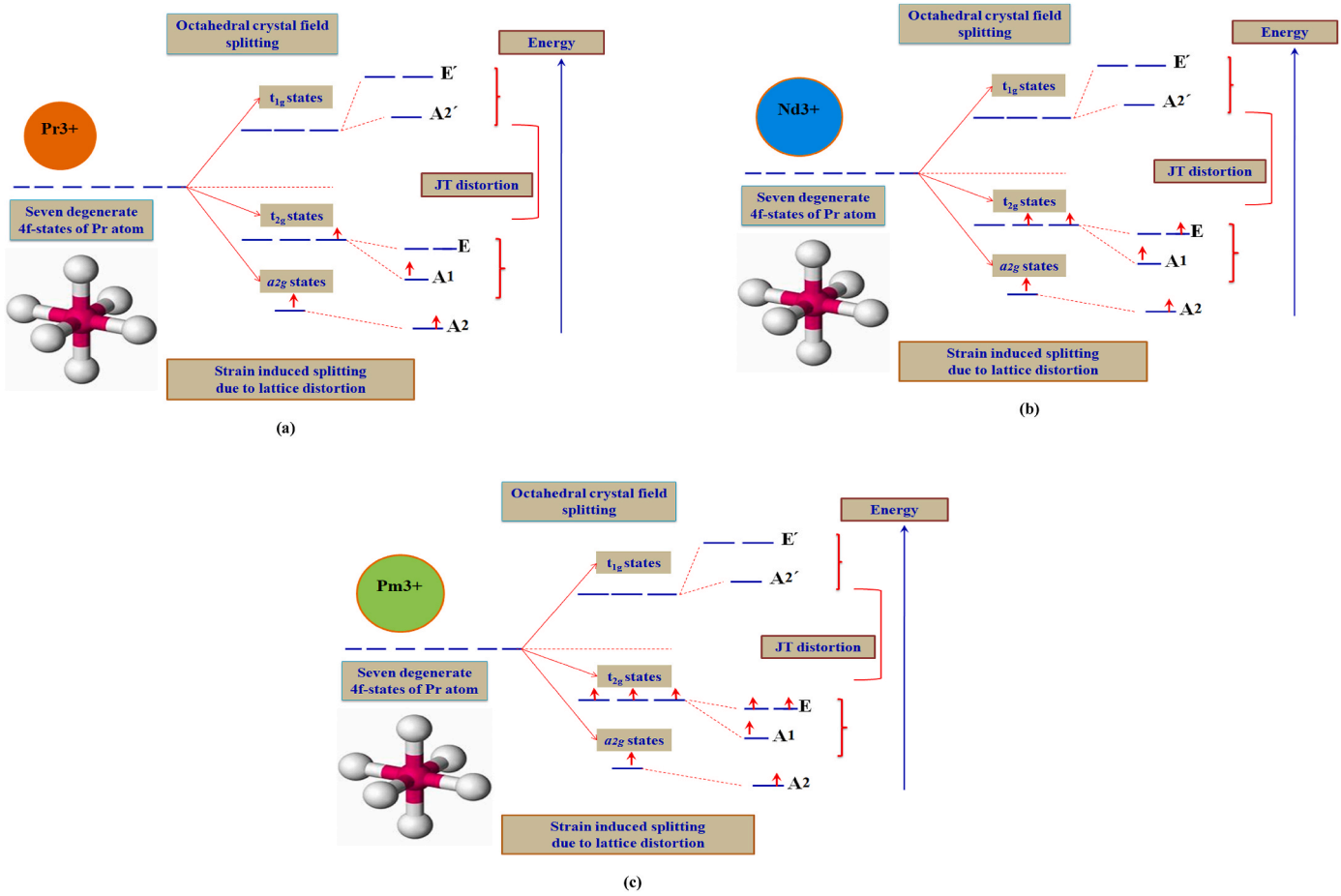

Fig. 5(a). splitting mechanism of electronic distributions f-states of Pr^{+3}in t_{1g} and t_{2g} are the highest three folds degenerate energy states and a_{2g} is the lowest single-fold degenerate energy.
Fig. 5(b): splitting mechanism of electronic distributions *f*-states of Nd in t_{1g} and t_{2g} are the highest three folds degenerate energy states and a_{2g} is the lowest single-fold degenerate energy.
Fig. 5(c): splitting mechanism of electronic distributions f-states of Pm^{+3}in t_{1g} and t_{2g} are the highest three folds degenerate energy states and a_{2g} is the lowest single-fold degenerate energy.

Table 2
Total, partial magnetic moment and interstitial (μ_B), and interstitial magnetic moment (μ_B) in KXO_2 (X = Pr, Nd, and Pm) compounds.

Parameters	total (μ_B)	K (μ_B)	X (μ_B)	O (μ_B)	Interstitial (μ_B)
$KPrO_2$	5.01	−0.00028	4.851	0.087	0.082
$KNdO_2$	3.006	−0.01379	2.950	0.0850	−0.099
$KPmO_2$	3.996	−0.00149	3.911	−0.08394	0.171

conductivity of KXO_2 (X = Pr, Nd, and Pm). For $KPmO_2$, it increases as does the electrical conductivity with increasing temperature which further reveals that low charge carriers move from VB to CB and produce less thermal agitation due to the wide band gap (4 eV) of $KPmO_2$. Whereas, in the case of $KPrO_2$ and $KNdO_2$, the thermal conductivity is low as compared to $KPmO_2$. As the band gap values of $KPrO_2$ and $KNdO_2$ are low than $KPmO_2$, hence a large number of charge carriers shift from VB to CB which produce higher thermal agitation [38,39]. Therefore, $KPrO_2$ and $KNdO_2$ have less values of thermal conductivity.

A combined impact of the electron, phonon, and heat absorption in semiconductor materials is described by specific heat capacity (C_v) [4]. Fig. 7(b) indicates the heat capacity of these materials. The heat capacity of $KPmO_2$ is increased linearly with increasing temperature. The graph of heat capacity for $KPmO_2$ obeys the Debye temperature relation, i.e., $C_v \propto T^3$ [5,6]. While, for $KNdO_2$, heat capacity is higher than $KPmO_2$ and $KPrO_2$ which unveils that it has a higher ability to absorb heat.

The temperature-dependent parameter such as magnetic susceptibility (χ) is concerned with the magnetic response of any materials against the applied magnetic field [7]. The plots of χ for KXO_2 (X = Pr, Nd, and Pm) are depicted in Fig. 7(c). Initially, all compounds, i.e., KXO_2 (X = Pr, Nd, and Pm) show the positive values of their χ, which however, descends linearly with the increasing temperature range from 100 K to 800 K. The shifting of its positive value towards zero or negative value of magnetic susceptibility reflects the nonmagnetic behavior [8]. It is noticed from Fig. 7(c) that these studied materials have magnetic behavior owing to have positive value of magnetic susceptibility. Finally, efficiency of the thermoelectric devices is described by figure of merit (ZT) [9,10]. ZT results are shown in Fig. 7(d). It is clear that the ZT value of $KPmO_2$ linearly increased with increasing temperature due to the combined effect of σS^2T. In the case of $KNdO_2$ value of ZT is also increased linearly with increasing temperatures beyond 500 K temperature. Where, in the case of $KPrO_2$, ZT becomes constant at 500 K temperature due to the constant value of the Seebeck coefficient. $KPmO_2$ has a greater value of ZT than $KNdO_2$ and $KPrO_2$ which can be a potential material for thermoelectric applications [17,18].

4. Conclusions

In this manuscript, the structural, electronic band gap structure for both spins and DOS, and magnetic properties of KXO_2 (X = Pr, Nd, and Pm) compounds are implemented by first-principles study in WIEN2K

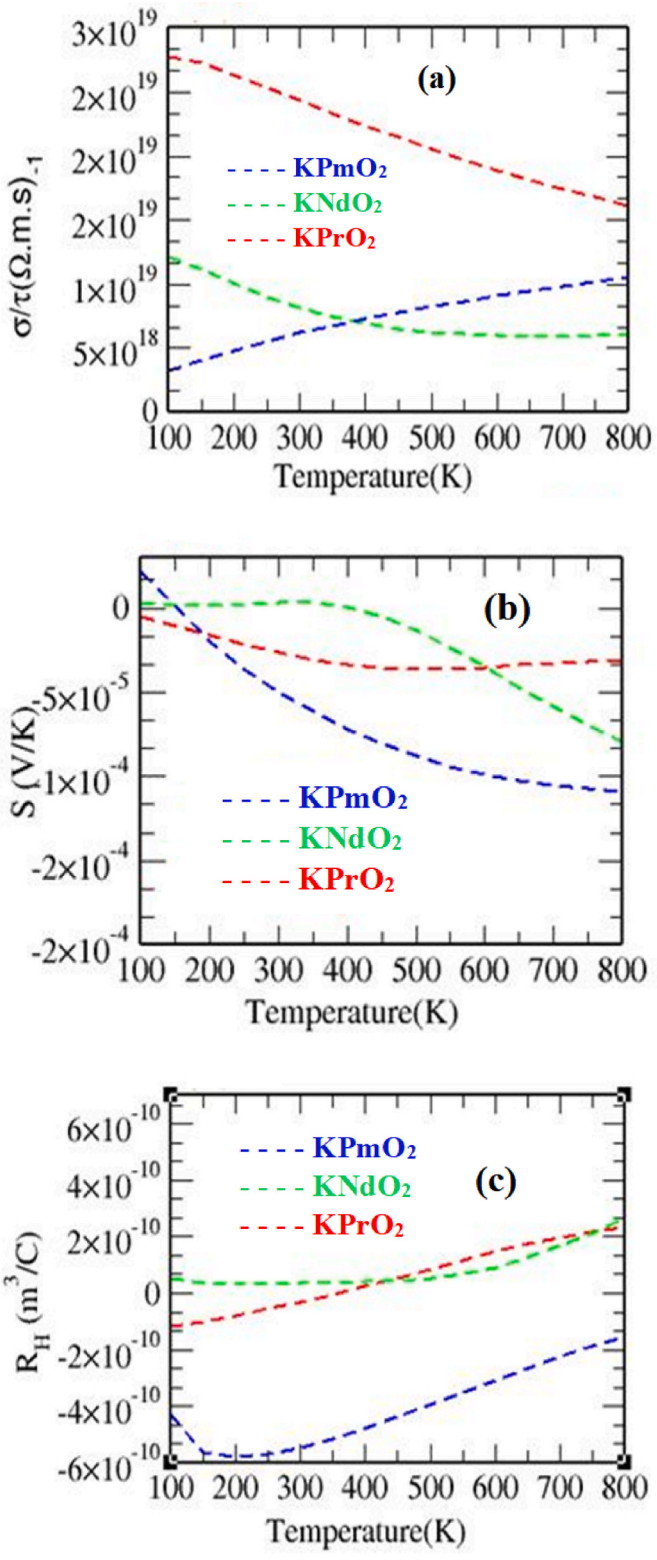

Fig. 6. Plots results (a) electrical conductivity (b) Seebeck coefficient (c) Hall Coefficient.

software, and thermoelectric properties are computed by Boltzmann transport theory. Direct electronic band gaps of 2.62 eV, 3.34 eV, and 4.0 eV were predicted for $KPrO_2$, $KNdO_2$, and $KPmO_2$, respectively. Moreover, half metallicity has been determined while analyzing spin channels. One channel has shown metallic nature, whereas, the other one has reflected the semiconducting behavior of these compounds. In addition, the total magnetic moments are found to be integers that confirmed half metallicity of these materials. The results show that being 100% spin polarization at the Fermi level, these potassium-based lanthanide oxides play a key role in spintronics devices closer to the realm of practical applications. The ZT value is higher for $KPmO_2$ as compared to $KNdO_2$ and $KPrO_2$ which has shown its increasing trend on increasing temperature. Thus, the predicted thermoelectric results have declared $KPmO_2$ a more promising candidate for thermoelectric applications than the other two compounds.

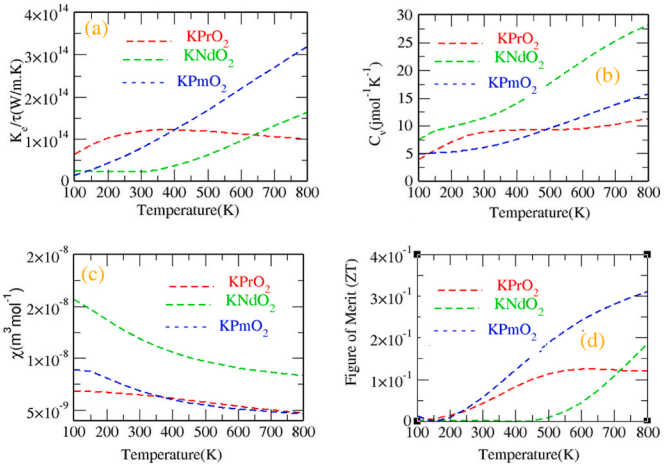

Fig. 7. Plots results (a) thermal conductivity (b) Specific Heat Capacity (c) magnetic susceptibility (d) Figure of merit.

Authors contributions

Conceptualization, G. Murtaza; **Methodology,** G. Murtaza, Khawar Ismail, Muhammad Iqbal Hussain; **Software,** G. Murtaza, **Validation,** G. Murtaza, R. M. Arif Khalil, and Muhammad Iqbal Hussain; **Formal Analysis,** G. Murtaza, R. M. Arif Khalil, Muhammad Iqbal Hussain, and Hassan Ali; **Investigation**, Khawar Ismail, and Samia Razzaq; **Resources,** Muhammad Iqbal Hussain, and Khawar Ismail; **Data Curation,** Khawar Ismail, and Bisma Tariq; **Writing-Original Draft Preparation,** Khawar Ismail, Muhammad Iqbal Hussain **Writing-Review & Editing,** G. Murtaza, Muhammad Iqbal Hussain, Khawar Ismail, Ghazanfir Nazir, Nouf H. Alotaibi, and Bisma Tariq **Visualization,** G. Murtaza, Khawar Ismail, Muhammad Iqbal Hussain, and R. M. Arif Khalil; **Supervision,** G. Murtaza; Funding **Acquisition**, No.

Declaration of competing interest

The authors declare that they have no known competing financial interests or personal relationships that could have appeared to influence the work reported in this paper.

Data availability

Data will be made available on request.

References

[1] S.A. Chambers, Y.K. Yoo, New materials for spintronics, MRS Bull. 28 (10) (2003) 706–710.
[2] K. Ismail, H. Albalawi, G. Murtaza, T.I. Al-Muhimeed, A.A. AlObaid, Q. Mahmood, Study of half-metallic ferromagnetism, transport and mechanical properties of X0.9375Ti0.0625Te (X= Ca, Sr, and Ba) alloys: for spintronics application, Phys. Scripta 96 (9) (2021), 095802.
[3] M. Dehghanzadeh, F. Ahmadian, Half-metallicity and magnetism of the full-Heusler compounds KYX2 (Y= Ti, V, and Cr; X= C, N, and O), Solid State Commun. 251 (2017) 50–59.
[4] N. Yaqoob, B. Sabir, G. Murtaza, R.M. Arif Khalil, N. Muhammad, A. Laref, Structural, electronic, magnetic, optical and thermoelectric response of half-

metallic AMnTe2 (A= Li, Na, K): an ab-initio calculations, Phys. B Condens. 574 (2019) 1–10.
[5] M. Mouatassime, Y. Selmani, S. Idrissi, L. Bahmad, F. Goumrhar, H. Labrim, A. Benyoussef, Magnetic properties and half metallic behavior of the Full-Heusler Co2FeGe alloy: DFT and Monte Carlo studies, J. Solid State Chem. 304 (2021) 1–8.
[6] N. Yaqoob, G. Murtaza, M.W. Iqbal, N.A. Noor, A. Mahmood, S.M. Ramay, W. Al-Masry, N.Y. Al-Garadi, Study of half-metallic nature and transport properties of XMnSe2 (X= Ca, Sr, and Ba) compounds via ab-initio calculations, J. Mater. Res. Technol. 9 (5) (2020) 10511–10519.
[7] A.G. El Hachimi, H. Zaari, A. Benyoussef, M. El Yadari, A. El Kenz, First-principles prediction of the magnetism of 4f rare-earth-metal-doped wurtzite zinc oxide, J. Rare Earths 32 (8) (2014) 715–721.
[8] M. Chepkoech, D.P. Joubert, G.O. Amolo, Theoretical investigation of the thermoelectric properties of ACuO2 (A= K, Rb and Cs), Eur. Phys. J. B93 (2020) 1–12.
[9] D. Bin, Y. Doi, Y. Hinatsu, Structure and magnetic properties of ternary potassium lanthanide oxides KLnO2 (Ln= Y, Nd, Sm–Lu), J. Alloys Compd. 453 (1–2) (2008) 282–287.
[10] A. Benmakhlouf, A. Bentabet, A. Bouhemadou, S. Maabed, A. Benghia, R. Khenata, S. Bin-Omran, Structural, half-metallic magnetism and elastic properties of the KMnQ2 (Q= O, S, Se, Te) chalcogenides from first-principles calculations, J. Magn. Magn Mater. 408 (2016) 199–205.
[11] M. Mushtaq, A. Muhammad, A. Ali, M.A. Sattar, S. Muhammad, First-principles search for half-metallic ferromagnetism in CsCrZ2 (Z=O, S, Se or Te) Heusler alloys, J. Mol. Graphics Modell. 98 (2020) 1–20.
[12] S. Ghosal, H. Luitel, S.K. Mandal, D. Sanyal, D. Jana, Half metallic ferromagnetic and optical properties of ruthenium-doped zincblende ZnS: a first-principles study, J. Phys. Chem. Solid. 136 (2020) 1–8.
[13] Z.H. Zhu, X.H. Yan, Half-metallic properties of perovskite BaCrO3 and BaCr0.5Ti0.5O3 superlattice: LSDA+U calculations, J. Appl. Phys. 106 (2) (2009) 1–5.
[14] A. Labdelli, A. Boukorrt, S. Meskine, H. Abbassa, A. Zaoui, Investigation of optoelectronic and thermoelectric properties of half-metallic BaRuO3 using DFT+U, Int. J. Comput. Mater. Sci. Eng. 7 (3) (2018) 1–18.
[15] G. Vaitheeswarana, V. Kanchana, A. Delin, Pseudo-half-metallicity in the double perovskite Sr2CrReO6 from density-functional calculations, Appl. Phys. Lett. 86 (2005) 1–3.
[16] K. Ismail, G. Murtaza, S. Tahir, G. Nazir, N.A. Kattan, H. Albalawi, B. Ul Haq, M. Morsi, Theoretical study of electronic, magnetic, optical and thermoelectric properties of XMnO2 (X= Au, Ag, Cu) oxides by DFT, Solid State Chem 314 (2022) 123–132.
[17] M. Shakil, S. Mushtaq, I. Zeba, S.S.A. Gillani, M.I. Khan, H. Arshad, M. Rafique, Structural, electronic, magnetic and thermoelectric properties of full Heusler alloys Co2YZ (Z= S, Ge, Se): a first-principles calculation, Phys. B Condens. 602 (1) (2021) 1–35.
[18] U. Hayat, S. Khalid, Exchange interactions, half-metallic ferromagnetism, mechanical, thermal and magneto-electronic properties of full Heusler alloys Co2YGe (Y= Mn, Fe) for acoustical and spintronic devices, Phys. B Condens. 615 (15) (2021) 1–12.
[19] M.K. Butt, M. Yaseen, J. Iqbal, A.S. Altowyan, A. Murtaza, M. Iqbal, A. Laref, Structural, electronic, half–metallic ferromagnetic and optical properties of cubic MAlO3 (M= Ce, Pr) perovskites: a DFT study, J. Phys. Chem. Solid. (2021) 1–7.
[20] Q. Mahmood, M. Rashid, B. Amin, N.A. Noor, A. Laref, Theoretical prediction of optoelectronic and thermoelectric properties of RbXO2 (X= Al, Ga, In) for renewable energy applications, Chem. Phys. Lett. 728 (2019) 87–93.
[21] Z. Charifi, H. Baaziz, F.E.H. Hassan, N. Bouarissa, High-pressure study of structural and electronic properties of calcium chalcogenides, J. Phys. Chem. Solid. 17 (26) (2005) 1–10.
[22] D. Srivastava, G.C. Tewari, M. Karppinen, R.M. Nieminen, First-principles study of layered antiferromagnetic CuCrX2 (X= S, Se and Te), J. Condens. Matter Phys. 25 (10) (2013) 1–6.
[23] M.A. Marquardt, N.A. Ashmore, D.P. Cann, Crystal chemistry and electrical properties of the delafossite structure, Thin Solid Films 496 (1) (2006) 146–156.
[24] A. Gencer, G. Surucu, Investigation of structural, electronic and lattice dynamical properties of XNiH3 (X= Li, Na, and K) perovskite type hydrides and their hydrogen storage applications, Int. J. Hydrogen Energy 44 (29) (2019) 15173–15182.
[25] N.A. Noor, M.W. Iqbal, T. Zelai, A. Mahmood, H.M. Shaikh, S.M. Ramay, W. Al-Masry, Analysis of direct band gap A2ScInI6 (A= Rb, Cs) double perovskite halides using DFT approach for renewable energy devices, J. Mater. Res. Technol. 13 (2021) 2491–2500.
[26] A.S. Oreshonkov, N.O. Azarapin, N.P. Shestakov, S.V. Adichtchev, Experimental and DFT study of BaLaCuS3: direct band gap semiconductor, J. Phys. Chem. Solid. 148 (2021) 1–7.
[27] Z. Zada, R. Zada, A.A. Khan, M. Saqib, M.F.Ur Rehman, M. Ismail, N. Kulhari, K. S. Sharma, X. Shen, M. Faizan, Investigation of electronic structure, magnetic stability, spin coupling, and thermodynamic properties of novel antiferromagnets XMn2Y2 (X= Ca, Sr; Y= P, as), J. Mol. Struct. 1268 (2022), 133698.
[28] G. Zhao, M. Xu, C. Zhao, S. Li, Q. Gong, Y. Hang, Improved performance of Faraday effect based on Pr3+, Ce3+ co-doped terbium gallium garnet crystal, Opt. Commun. 506 (1) (2022), 127587.
[29] M. Ju, X. Kuang, C. Lu, H. Li, J. Wang, C. Zhang, Y. Zhu, Y. Yeung, Determination of the microstructure, energy levels and magnetic dipole transition mechanism for Tm3+ doped yttrium aluminum borate, J. Mater. Chem. C4 (10) (2016) 1988–1995.
[30] H.C. Kandpal, G.H. Fecher, C. Felser, Calculated electronic and magnetic properties of the half-metallic, transition metal based Heusler compounds, J. Phys. D Appl. Phys. 40 (6) (2007) 1507–1523.
[31] A. Marjaoui, M.A. Tamerd, M. Zanouni, A. El Kasmi, M. Diani, Electronic structure, optical and thermoelectric properties of Ge2SeS monolayer via first-principles study, Physica E Low Dimens. Syst. Nanostruct. 136 (2022), 115022.
[32] K. Morrison, F.K. Dejene, Thermal imaging of the thomson effect, Phys 13 (2020) 1–3.
[33] S. Kumar, N. Kumar, K. Yadav, A. Kumar, R.P. Singh, DFT investigations on optoelectronic spectra and thermoelectric properties of barium cadmium disulfide (BaCdS2), Optik 207 (2020) 1–23.
[34] R.B. Behram, M.A. Iqbal, S.M. Alay-e-Abbas, M. Sajjad, M. Yaseen, M.I. Arshad, G. Murtaza, Theoretical investigation of mechanical, optoelectronic and thermoelectric properties of BiGaO3 and BiInO3 compounds, Mater. Sci. Semicond. Process. 41 (2016) 297–303.
[35] S. Mondal, C. Mazumdar, R. Ranganathan, E. Alleno, P.C. Sreeparvathy, V. Kanchana, G. Vaitheeswaran, Ferromagnetically correlated clusters in semimetallic Ru2NbAl Heusler alloy and its thermoelectric properties, Phys. Rev. B 98 (20) (2018) 1–11.
[36] J. Mizusaki, T. Sasamoto, W.R. Cannon, H.K. Bowen, Electronic conductivity, Seebeck coefficient, and defect structure of LaFeO3, J. Am. Ceram. Soc. 65 (8) (1982) 363–368.
[37] Md.M. Islam, M.O. Liedke, D. Winarski, M. Butterling, A. Wagner, P. Hosemann, Y. Wang, B. Uberuaga, F.A. Selim, Chemical manipulation of hydrogen induced high *p*-type and *n*-type conductivity in Ga_2O_3, Sci. Rep. 10 (1) (2020) 1–10.
[38] C. Shen, N. Hadaeghi, H.K. Singh, T. Long, L. Fan, G. Qin, H. Zhang, Two-dimensional buckling structure induces the ultra-low thermal conductivity: a comparative study of the group GaX (X= N, P, As), J. Mater. Chem. C10 (4) (2022) 1436–1444.
[39] A. Puzari Merangmenla, Microwave-induced synthesis of a new benzodiazepinone based chemosensor in chloroform under thermal agitation: a potential fluorescent sensor for multi-signaling detection of metal ions, Inorg. Chim. Acta. 505 (2020) 1–8.